Ionics (2021) 27:4135–4142
https://doi.org/10.1007/s11581-021-04193-9

ORIGINAL PAPER

High-voltage $LiNi_{0.4}Co_{0.4}Mn_{0.2}O_2$/graphite pouch battery cycled at 4.5 V with a LiDFP-based electrolyte

Chengyun Wang[1,2] · Mingyao Liu[1] · Donghai Huang[1] · Qingquan Wang[1] · Ao Mei[1] · Weizhen Fan[4] · Jianshan Ye[2] · Wei Yang[3]

Received: 31 December 2020 / Revised: 22 June 2021 / Accepted: 17 July 2021 / Published online: 24 July 2021

Abstract

Increasing the charging cutoff voltage is an effective method for improving the energy density of lithium-ion batteries. However, the conventional carbonate-based electrolyte with $LiPF_6$ is unstable when the end-of-charge voltage up to 4.5 V (vs. Li/Li^+), resulting in poor cycling stability of LIBs. In this work, when 1.0 wt% LiDFP is added into the conventional electrolyte for $LiNi_{0.4}Co_{0.4}Mn_{0.2}O_2$/graphite pouch cells, the capacity retention of the cell is significantly improved from 22.9 to 87.6% after 100 cycles, even a high capacity retention of 81.0% is maintained after 200 cycles. The results of spectroscopic and electrochemical techniques indicate that the passivation film induced by LiDFP can be formed simultaneously at both cathode and anode surfaces. The improvement of cell high-voltage performance can be credited to the addition of LiDFP, which effectively inhibited the dissolution of transition metals and the side reaction of electrolyte on the cathode and anode surfaces.

Keywords Lithium-ion batteries · High voltage · Electrolyte · LiDFP · Additive

Introduction

With the development of new energy automobile industry, lithium-ion batteries (LIBs) are being widely favored in the field of electric vehicles owing to their advantages of high-energy density, rechargeable ability, and long repeat service life [1–5]. As the core component of electric vehicle power system, the performances of LIBs directly determine the driving range and the market competitiveness of electric vehicles. Therefore, the advanced of LIB technology with good safety performance, higher energy density, and low production cost is urgent to promote the development of the new energy electric automobile industry.

The energy density of LIBs is highly cathode materials dependent, and the ternary layered $LiNi_xCo_yMn_{1-x-y}O_2$ (NCM, $0 < x, y < 1$) has considered as a prominent cathode material owing to their high operating voltage and high capacity. To meet the demands for electric vehicle applications, raising the end-of-charge voltage can increase the specific capacity of these materials and provide a higher energy density for the LIBs [6–8]. The traditional electrolyte is mainly composed of lithium hexafluorophosphate ($LiPF_6$) as the solute and organic carbonate/carboxylate as the solvent, which is closely related to the performance of cells. For example, while the operating voltage is greater than 4.5 V (vs. Li/Li^+), the electrolyte suffers severe oxidation decomposition on the cathode, which cannot meet the requirement of normal working for those cathode materials under the high voltage [9, 10]. Furthermore, the decomposition of electrolyte is accompanied by the hydrogen fluoride (HF) generation. HF will corrode the cathode materials, causing the dissolution of transition metal ions (such as, Ni, Co, and Mn) in cathode materials, and further migration,

Chengyun Wang and Mingyao Liu contributed equally to this work.

✉ Qingquan Wang
wangqingquan@gacrnd.com

✉ Wei Yang
wyang@gzhu.edu.cn

[1] GAC Automotive Research & Development Center, Guangzhou 511400, Guangdong, China

[2] School of Chemistry and Chemical Engineering, South China University of Technology, Guangzhou 510000, Guangdong, China

[3] School of Chemistry and Chemical Engineering, Guangzhou University, Guangzhou 511400, Guangdong, China

[4] Guangzhou Tinci Materials Technology Co. Ltd., Guangzhou 510760, China

and deposition between cathode and anode surface. These issues would trigger the sustained electrolyte decomposition as well as lithium dendrites growth on the anode [11]. Therefore, it is significantly important to develop suitable electrolytes that meet the high-voltage requirements of $LiNi_xCo_yMn_{1-x-y}O_2$-based cells.

Changing the electrolyte components (solvents and additives) is the most convenient strategy to improve the electrochemical performance of cells at high voltage. Although some high-voltage solvents, such as fluorinated, sulfones, and room temperature ionic liquids (RTILs), can deliver a wider electrochemical window for electrolytes, those solvents suffer from the poor lithium salt solubility and high viscosity, which will sacrifice the rate capability and low-temperature performance of cells [12–15]. Additives occupy a small proportion in the electrolyte and generally have little effect on the physicochemical characteristics of the electrolyte. Therefore, it is a practical and effective method to improve the performances of the cells by adding some additives into the electrolyte. Recently, functional electrolyte additives like L-tryptophan [16], 2-(trifluoroacetyl) thiophene [17], and trimethyl borate [18] have been reported for enhancing the electrochemical performance of cells at high voltage and their cathode film-forming properties. However, the effect of these additives on the surface interface of the anode has been rarely reported. Meanwhile, those organic electrolytes will consume the active lithium in the process of interface formation, resulting in reduced Coulombic efficiency and even a negative impact on the initial cycle capacity of the battery.

As an electrolyte additive, lithium difluorophosphate (LiDFP) has been extensively investigated in commercial NCM/graphite full cells to improve the low-temperature performance [19], improve the high-voltage performance [20, 21], decrease the internal impedance, and enhance rate performance [22, 23]. Additionally, LiDFP also has been confirmed as an effective electrolyte component for lithium metal batteries [24, 25]. These works indicated that LiDFP is a multifunctional additive by forming a stable surface film with high ionic conductivity on different electrodes. For the ternary layered NCM cathode material, the proportions of Ni, Co and Mn in these materials will result in a difference in surface interface properties. Although LiDFP has shown positive effect on other NCM-based battery systems, the application of LiDFP in the $LiNi_{0.4}Co_{0.4}Mn_{0.2}O_2$ material-based cell has been rarely studied. In this work, to further confirm the general adaptability of LiDFP as an efficient electrolyte additive, the $LiNi_{0.4}Co_{0.4}Mn_{0.2}O_2$/graphite pouch cells are used to test the effect of LiDFP on the high-voltage performance. Electrochemical results show that LiDFP can improve the rate capacity and cycling stability of $LiNi_{0.4}Co_{0.4}Mn_{0.2}O_2$/graphite pouch cells under the end-of-charge voltage of 4.5 V. Microscopic characterizations further validate that addition of LiDFP inhibits the dissolution and deposition of transition metal ions, constrains the continuous decomposition of electrolyte by passivating the interface between cathode and anode surfaces, and subsequently improves the high-voltage performance.

Experiment section

Preparation of electrode and electrolyte

The graphite materials and $LiNi_{0.4}Co_{0.4}Mn_{0.2}O_2$ were provided by BTR Battery Materials Co., Ltd., and Shenzhen Tianjiao Technology Co., Ltd., respectively. The positive electrode slurry using N-methyl-2pyrrolidinone (NMP) as dispersion solvent is composed of $LiNi_{0.4}Co_{0.4}Mn_{0.2}O_2$, poly(vinylidenedifluoride) (PVDF), and conductive carbon (weight ratio 93.0: 4.0: 3.0). The negative electrode slurry is composed of graphite, styrene butadiene rubber (SBR), carboxymethyl cellulose (CMC), and Super-P (weight ratio 95.0: 2.5: 1.5: 1.0), in which the deionized water was used as the dispersion solvent. Afterwards, the two slurries were cast onto the Al foil and Cu foil, respectively, and then putted into a vacuum drying oven to dry at 120 °C for around 12 h. The average loading level of the prepared cathode and anode electrode was 31.80 and 16.55 mg cm^{-2}, respectively. The dried $LiNi_{0.4}Co_{0.4}Mn_{0.2}O_2$ electrode, graphite electrode, and Celgard 2400 separator were rolled up and then put into the specific aluminum-plastic to obtain the cells without electrolyte. For the $LiNi_{0.4}Co_{0.4}Mn_{0.2}O_2$/graphite cells at 4.2 V and 4.5 V, the capacities of these cells are designed about 550 and 665 mAh, and the capacity ratios of anode to cathode electrode (N/P ratios) are about 1.30 and 1.15, respectively.

The battery-grade $LiPF_6$, LiDFP, diethyl carbonate (DEC), ethylene carbonate (EC), and dimethyl carbonate (DMC) solvent were supplied by Guangzhou Tinci Materials Technology Co., Ltd. and without further purification. One molar $LiPF_6$ dissolved in EC and DEC (weight ratio 1:3) preparing in a glove box filled with Ar was used as reference electrolyte, where the moisture and oxygen contents were controlled lower than 1.0 ppm. Different contents (0.5%, 1.0%, 1.5%, and 2.0%, wt%) of LiDFP were dissolved in the reference electrolyte and were used as the studied electrolytes. The moisture and free acid contents of the electrolytes were measured by auto moisture titration instrument (KF 831 Metrohm, Swiss) and automatic potentiometric titrator (798 Metrohm, Swiss), and the corresponding contents were kept below 50.0 ppm and 20.0 ppm. The $LiNi_{0.4}Co_{0.4}Mn_{0.2}O_2$/graphite pouch cells with different

electrolytes were assembled in the glove box, and the electrolyte injection weight is maintained at about 3.65 ± 0.05 g for each cell.

Electrochemical and surface characterizations

All charge/discharge tests were measured on the Neware cell testing system (CT-3008) at room temperature. The $LiNi_{0.4}Co_{0.4}Mn_{0.2}O_2$/graphite pouch cells of the 1st, 2nd, and 3rd cycles were conducted galvanostatically at 0.1 C, 0.2 C, and 1.0 C, respectively. Subsequently, the cycling performance of the pouch cells was tested at a constant current of 1.0 C at voltage ranges of 3.0–4.2 V and 3.0–4.5 V. The rate performance was carried in a content charging current of 1.0 C and then discharged at 0.2 C, 0.5 C, 1.0 C, 2.0 C, 3.0 C, and 5.0 C in the voltage ranges of 3.0–4.5 V, respectively. Measurements at each C-rate were repeated over 5 cycles. The electrochemical impedance measurement was performed at the charged state over the limited frequency range (100 kHz to 40 mHz) and amplitude potential (10 mV) on a frequency response analyzer (Solartron1455A, England). For surface characterizations, the cells after the charge/discharge cycles were disassembled manually inside a glove box. The $LiNi_{0.4}Co_{0.4}Mn_{0.2}O_2$ and graphite electrode were rinsed with battery-grade DMC for three times and thoroughly dried under a vacuum drying oven at room temperature. The field emission scanning electron microscopy (SEM, ZEISS Ultra 55, Germany) was used to observe the surface morphologies of the fresh and cycled electrodes. The energy dispersive spectrometer (EDS, Bruker Quantax 200, Germany) was used to analyze the surface element content of the cathode and anode electrodes.

Results and discussion

Electrochemical performances

To explore the influence of LiDFP as an additive in the electrolyte on the electrochemical performance at high voltage, the cycling performance of $LiNi_{0.4}Co_{0.4}Mn_{0.2}O_2$/graphite pouch cells containing different amount of LiDFP was studied at various end-of-charge voltages (4.2 and 4.5 V). All cells were charged and discharged under a constant current density of 1.0 C. As shown in Fig. 1a and Table 1, the cyclic performance of the LiDFP-containing unit cell is significantly improved; the capacity of LiDFP-free unit cell decays sharply and exhibits a capacity retention of 22.9% (the initial discharge capacity was 159.8 mA h g^{-1} and decreased to 36.6 mA h g^{-1} after 100 cycles) after the 100th cycle. By contrast, the corresponding capacity retention of the cell containing 0.5% and 1.0% content of LiDFP in the electrolyte maintained 86.4% (the initial discharge capacity was 159.9 mA h g^{-1} and decreased to 138.1 mA h g^{-1} after

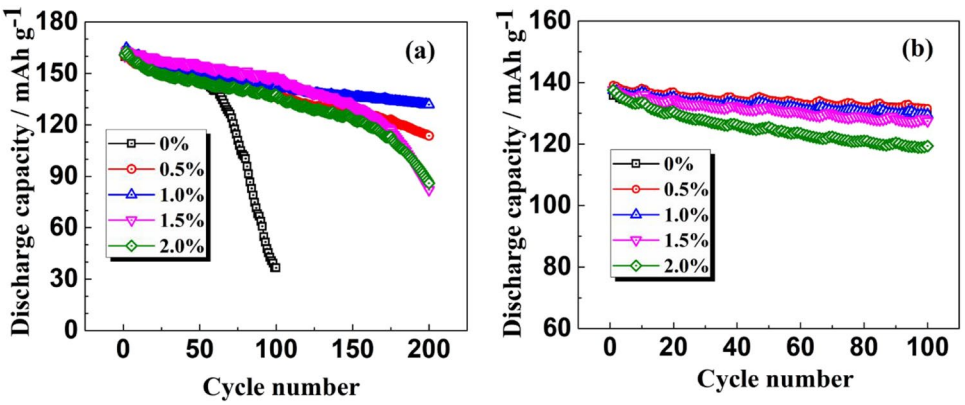

Fig. 1 The effect of LiDFP on the cyclic performance of $LiNi_{0.4}Co_{0.4}Mn_{0.2}O_2$/graphite cells operated at different end-of-charge voltages of (**a**) 4.5 V and (**b**) 4.2 V

Table 1 Discharge capacities and discharge capacity retentions of the $LiNi_{0.4}Co_{0.4}Mn_{0.2}O_2$/graphite pouch cells contained different weight ratios of LiDFP in the electrolyte beyond the end-of-charge voltages of 4.2 and 4.5 V after 100 and 200 cycles

Potential range		0%	0.5%	1.0%	1.5%	2.0%
3.0–4.2 V (100th)	Discharge capacity (1st)	135.8	139.1	137.5	137.6	137.5
	Discharge capacity (100th)	130.5	131.6	129.5	127.5	119.4
	Capacity retention (100th)	96.1%	94.5%	94.2%	92.6%	86.8%
3.0–4.5 V (100th)	Discharge capacity (1st)	159.8	159.9	162.8	160.2	160.8
	Discharge capacity (100th)	36.6	138.1	142.6	146.8	137.4
	Capacity retention (100th)	22.9%	86.4%	87.6%	91.6%	85.4%
3.0–4.5 V (200th)	Discharge capacity (200th)	—	113.6	131.9	82.2	86.0
	Capacity retention (200th)	—	71.0%	81.0%	51.3%	53.5%

100 cycles) and 87.6% (the initial discharge capacity was 162.8 mA h g^{-1} and decreased to 142.6 mA h g^{-1} after 100 cycles) of the initial discharge capacity, respectively. There is no significant difference in the capacity loss among the cells containing 0.5% and 1.0% LiDFP after 100 cycles. As the cycle progressed, when the cell cycles 200 times, the cell containing 1.0% of LiDFP showed the most excellent cyclic stability with a capacity retention of about 81.0% (131.9 mA h g^{-1} after 200 cycles), while the cell with 0.5% of LiDFP only maintained 71.0% of the initial discharge capacity (113.6 mA h g^{-1} after 200 cycles). Intriguingly, when the cells cycled at an end-of-charge voltage of 4.2 V, the cells used the electrolyte containing 0%, 0.5%, 1.0%, 1.5%, and 2.0% LiDFP display slight difference in cycling performance (Fig. 1b), as well as the capacity retention rates of the cells are 96.1%, 94.5%, 94.2%, 92.6%, and 86.8% after 100 cycles, as shown in Table 1. The cycling performance of the cells under different end-of-charge voltages is significantly different, indicating that LiDFP as an electrolyte additive for 4.5 V $LiNi_{0.4}Co_{0.4}Mn_{0.2}O_2$/graphite pouch battery is effective.

Figure 2a exhibits the rate capability of $LiNi_{0.4}Co_{0.4}Mn_{0.2}O_2$/graphite pouch cells using the electrolytes, which were dissolved with 0% and 1.0% LiDFP, in the limited potential range of 3.0–4.5 V at different discharge currents of 0.2 C, 0.5 C, 1.0 C, 2.0 C, 3.0 C, and 5.0 C. And the corresponding average discharge capacities of each current are provided in Table 2. As can be seen from Fig. 2a, the discharge capacity of the 1.0% LiDFP additive-added cell is slightly higher than that of the cell without additive, and the difference in capacity is more obvious under high discharge current. Compared with the electrolyte without LiDFP, the average discharge capacity at 5.0 C increases from 40.1 to 52.6 mAh g^{-1} by the addition of LiDFP, as displayed in Table 2. The result shows that LiDFP enhances the capacity of the cell at high discharge current. The Coulombic efficiency of the $LiNi_{0.4}Co_{0.4}Mn_{0.2}O_2$/graphite cells cycling at rate of 1.0 C and in the operating voltage of 3.0–4.5 V for 200 cycles with 0% and 1.0% LiDFP is displayed in Fig. 2b. As seen from Fig. 2b, the Coulombic efficiency of LiDFP-free cell reaches the stable state need several cycles, while the addition of LiDFP could significantly shorten the stable period, indicating that LiDFP was more conducive to the formation of surface interface film. Additionally, the Coulombic efficiency of the cell employing the electrolyte containing 1.0% LiDFP displays very reposeful performance, which owns to the stable LiDFP-originated SEI film on the electrode surface, whereas the Coulombic efficiency of the LiDFP-free cell shows a sudden unpredictable change in cycling. This can come into a conclusion that the irregular change of the Coulombic efficiency is related with the formation and decomposition of the unstable SEI film, resulting in the loss of active substance. The successive decomposition of electrolyte on the electrode surface could hinder the de-intercalation/intercalation of Li^+ through electrode, resulting in capacity attenuation during cycling (Fig. 1a). Combined with the rate capability of cells in Fig. 2a, it can be explained that the interface membrane modified by LiDFP is relatively stable and is more conducive to Li^+ de-intercalation under high voltage.

The impedance measurements of the $LiNi_{0.4}Co_{0.4}Mn_{0.2}O_2$/graphite pouch cells were carried out to evaluate the effect of LiDFP additive. Nyquist plots of cells using electrolytes with 0% and 1.0% LiDFP additive

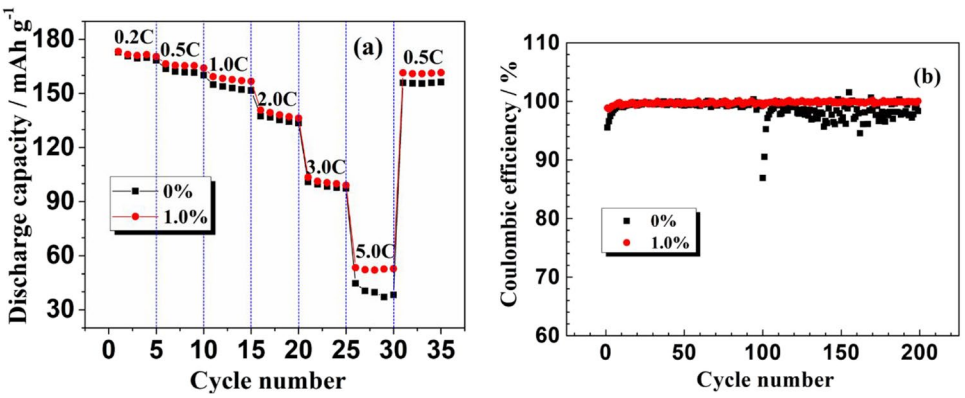

Fig. 2 $LiNi_{0.4}Co_{0.4}Mn_{0.2}O_2$/graphite cells with 0% and 1.0% LiDFP operated at 3.0–4.5 V: (**a**) rate performance and (**b**) Coulombic efficiencies at the charge/discharge rate of 1.0 C

Table 2 The average discharge capacity of $LiNi_{0.4}Co_{0.4}Mn_{0.2}O_2$/graphite cells with 0% and 1.0% LiDFP operated at 3.0–4.5 V under different charge/discharge rates

	Discharge capacity/mAh g^{-1}						
	0.2 C	0.5C	1.0 C	2.0 C	3.0 C	5.0 C	0.5 C
0%	170.3	161.9	153.1	135.5	98.8	40.1	155.8
1.0%	171.6	165.4	157.8	138.3	100.9	52.6	161.2

operated at 3.0–4.5 V before cycling and after 200 cycles are displayed in Fig. 3a and b, respectively. As can be seen in Fig. 3a, before cycling, there is a slight difference in the interfacial impedance between the cells with 0% and 1.0% LiDFP. Comparing to the additive-free cell, the impedance of the LiDFP-added cell is lower. The SEI film formed by LiDFP has a low interfacial impedance meaning and less migration resistance of Li^+, allowing the cells to have high Coulombic efficiency of the first cycle and good rate capability. However, the additive-free cell shows a rapidly enlarged semicircle during 200 cycles, as displayed in Fig. 3b. Figure 3c shows the equivalent circuit model, the high-frequency semicircle (R_f, surface-film resistance) and the intermediate frequency semicircle (R_{ct}, charge-transfer resistance) are two concerned parts of the EIS spectra of pouch cells [26–30], and the corresponding impedance spectrum fitting results are summarized in Table 3. For the cell without LiDFP additive, the values of R_f and R_{ct} are 110 and 601 mΩ, much higher than that of 57 and 103 mΩ for the LiDFP-added cell (Table 3). The change of EIS impedance is mainly determined by the character of interfacial film. An unstable SEI film will result in the continuous consumption of electrolyte; meanwhile, the accumulation of electrolyte decomposition products at the electrode interface is the major factor affecting the increase of cell impedance. In addition, the irreversible loss of active lithium in the electrolyte will directly cause the decline of the cell capacity. Combined with the above impedance measurements results, it can be inferred that LiDFP as an addictive is beneficial to enhance the stability of the surface film. Therefore, the LiDFP-originated SEI film can inhibit the side reactions on the electrode surface and alleviate the growth of the EIS impedance of cells during cycling at high voltage.

Table 3 Results of fitted impedance values for the $LiNi_{0.4}Co_{0.4}Mn_{0.2}O_2$/graphite pouch cells with 0% and 1.0% LiDFP after 200 cycles

Samples	Rf/mΩ	Rct/mΩ
0% LiDFP	110	601
1.0% LiDFP	57	103

Interface characterization

In order to further confirm the effect of LiDFP on the electrode interface, SEM and EDS characterizations were adopted to analyze the surface morphology and compositions of the circulating electrode. Figure 4a shows the SEM image of the pristine $LiNi_{0.4}Co_{0.4}Mn_{0.2}O_2$ electrode without electrolyte. It can be seen that the materials with a smooth surface and the contours between the particles are clear. Figure 4b and c exhibit the SEM images of the cycled $LiNi_{0.4}Co_{0.4}Mn_{0.2}O_2$ electrode with 0% and 1.0% LiDFP after 200 cycles, respectively. In comparison with the relatively clean particle surface of Fig. 4a, the surface of the cycled cathode without LiDFP is indefinable, suggesting that abundant electrolyte decomposition products accumulated. In contrast, in the electrolyte containing LiDFP, the circulating cathode electrode almost keeps the morphology of fresh cathode, verifying that the LiDFP layer film can effectively suppress the electrolyte decomposition. Table 4 displays the concentration of F, P, Ni, Co, and Mn on the surface of the cycled $LiNi_{0.4}Co_{0.4}Mn_{0.2}O_2$ and graphite electrode obtained from cells using 0% and 1.0% LiDFP by EDS characterization. From the element distribution of cathode surface, the contents of both F and P for the 1.0% LiDFP cell are lower than that in the cell with the additive-free electrolyte, as known that these two elements are mainly from $LiPF_6$ decomposition. The difference in the contents of F and P for the cells using different electrolytes indicates

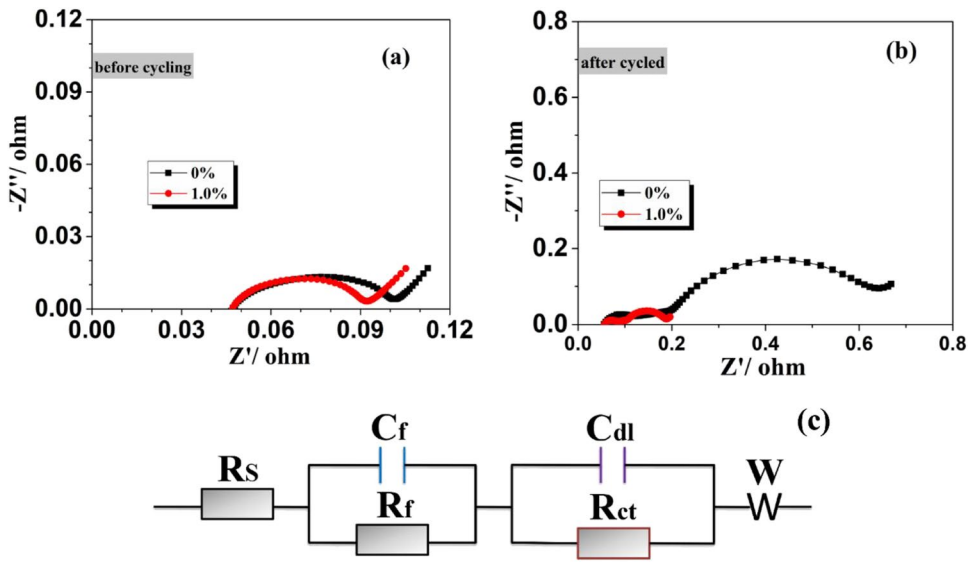

Fig. 3 EIS analysis of $LiNi_{0.4}Co_{0.4}Mn_{0.2}O_2$/graphite pouch cells with 0% and 1.0% LiDFP charged to 4.5 V: (**a**) before cycling; (**b**) after 200 cycles; (**c**) the corresponding equivalent circuit diagram

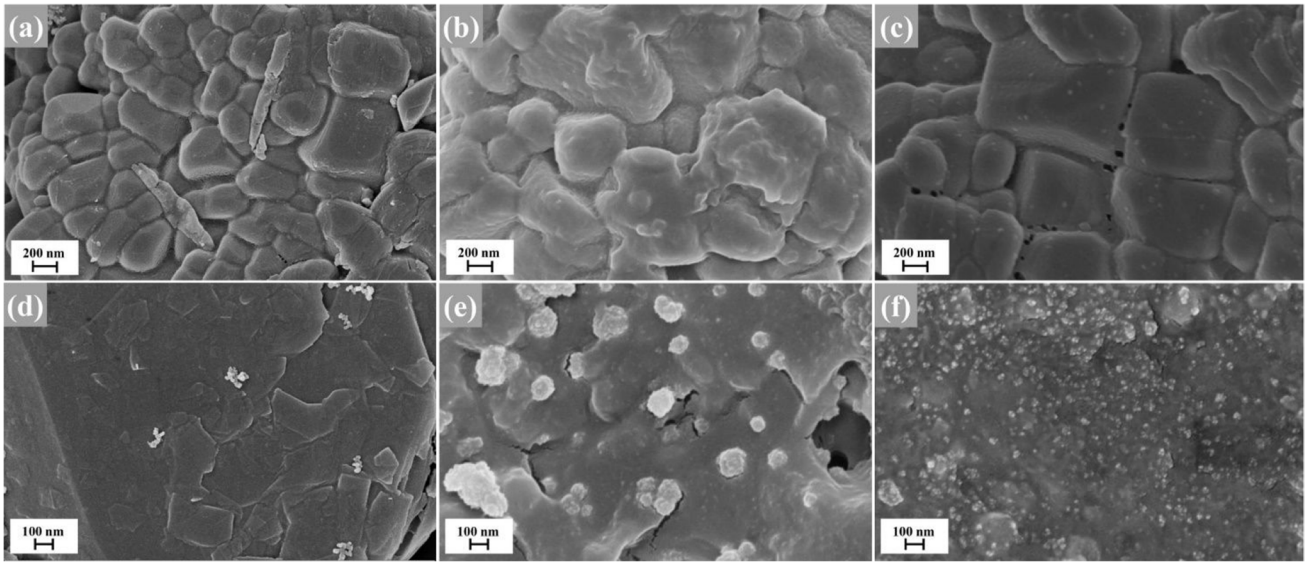

Fig. 4 SEM micrographs of fresh and the samples obtained from the $LiNi_{0.4}Co_{0.4}Mn_{0.2}O_2$/graphite pouch cells with 0% and 1.0% LiDFP cycled between 3.0 and 4.5 V after 200 cycles; cathode: (**a**) fresh, (**b**) 0% LiDFP, (**c**) 1.0% LiDFP; anode: (**d**) fresh, (**e**) 0% LiDFP, (**f**) 1.0% LiDFP

Table 4 Surface concentration of F, P, Ni, Co and Mn in the $LiNi_{0.4}Co_{0.4}Mn_{0.2}O_2$ and graphite electrodes gained from the cells added with 0% and 1.0% LiDFP in a limited operating voltage between 3.0 to 4.5 V after 200 cycles by EDS

		F	P	Ni	Co	Mn
		Atomic percent/at.%				
Cathode	0%	14.20	2.00	4.21	4.42	4.86
	1.0%	8.97	1.64	6.09	6.27	6.51
Anode	0%	23.45	3.95	0.08	0.16	0.40
	1.0%	14.99	3.69	0.03	0.07	0.17

that LiDFP as an additive can effectively protect the stability of electrolyte at the positive electrode surface. At the same time, the graphite electrode samples obtained under different conditions are also observed by SEM characterization, as displayed in Fig. 4d, e, and f. A fresh electrode, which is surrounded by PVDF (conductive agents), shows a clean surface (Fig. 4d), while the loop electrode in the electrolyte with 0% LiDFP is covered with thick deposits (Fig. 4e), and some obvious pores are presented in the coating layer, causing the direct contact between the electrode surface and the electrolyte. Differently, the circulating electrode in the electrolyte with 1.0% LiDFP displays a compact and uniform layer covered on the surface without visible gaps. Additionally, as can be seen from Table 4, the cell with 1.0% LiDFP shows a lower content of F and P than that of the additive-free cell, suggesting that 1.0% LiDFP added is effective in inhibiting the electrolyte from continuous decomposing during cell cycling. For the circulating cathode surface containing LiDFP, the Ni, Co, and Mn contents are higher than that of the sample without additive, which is caused by the formation of an interfacial protective film covering on the cathode surface by LiDFP. However, for the anode, the LiDFP-containing electrode surface delivers a lower Ni, Co, and Mn contents that the sample without additive, which indicates that the addition of LiDFP can effectively alleviate the dissolution of Ni, Co, and Mn from cathode and accumulate on the anode surface. Therefore, it can be seen from the SEM and EDS results that LiDFP can affect the morphology and chemical composition of both $LiNi_{0.4}Co_{0.4}Mn_{0.2}O_2$ and graphite surfaces and enhance the stability of SEI and CEI films. These microscopic characterization results are consistent with the electrochemical measurements.

Conclusions

LiDFP as a film-forming additive in $LiPF_6$/carbonate electrolyte greatly enhances the performance of $LiNi_{0.4}Co_{0.4}Mn_{0.2}O_2$/graphite pouch cells. Electrochemical results reveal that using the electrolyte with 1.0% LiDFP additive, the battery has significantly improved cycling performance at 4.5 V compared to that using additive-free electrolyte. The SEM and EDS results clearly show that the improvement of electrochemical performance at high

voltage is mainly attributed to its film-forming capability on the cathode and anode surfaces, which inhibits the serious electrolyte decomposition and the dissolution of transition metals. In addition, the modified electrode interface film by LiDFP has a low interface impedance, thus accelerating the Li^+ diffusion, and resulting in a high rate capability and Coulombic efficiency. This work demonstrates that LiDFP has prominent potential as functional additive for the development of high-energy density and high-voltage LIBs.

Funding This project funded by the China Postdoctoral Science Foundation (2020M682662), the Natural Science Foundations of Guangdong (No. 2018A030313423), and the Foundation for Innovative Research Groups of the National Natural Science Foundation of China (No. NSFC51621001).

References

1. Gu S, Cui Y, Wen K, Chen S, Zhao J (2020) 3-cyano-5-fluorobenzenzboronic acid as an electrolyte additive for enhancing the cycling stability of $Li_{1.2}Mn_{0.54}Ni_{0.13}Co_{0.13}O_2$ cathode at high voltage. J Alloys Compd 829:154491
2. Li X, Shi H, Zhang L, Chen J, Lü P (2020) Novel synthesis of SiOx/C composite as high-capacity lithium-ion battery anode from silica-carbon binary xerogel. Chin J Chem Eng 28:579–583
3. Zhou F, Yang X, Liu J, Liu J, Hu R, Ouyang L, Zhu M (2021) Boosted lithium storage cycling stability of TiP_2 by in-situ partial self-decomposition and nano-spatial confinement. J Power Sources 485:229337
4. Zhang M, Hu R, Liu J, Ouyang L, Liu J, Yang L, Zhu M (2017) A $ZnGeP_2$/C anode for lithium-ion and sodium-ion batteries. Electrochem Commun 77:85–88
5. Zhou F, Ouyang L, Liu J, Yang X, Zhu M (2020) Chemical bonding black phosphorus with TiO_2 and carbon toward high-performance lithium storage. J Power Sources 449:227549
6. Tao F, Yan X, Liu J, Lei H, Chen L (2016) Effects of PVP-assisted Co3O4 coating on the electrochemical and storage properties of $LiNi_{0.6}Co_{0.2}Mn_{0.2}O_2$ at high cut-off voltage. Electrochim Acta 210:548–556
7. Pham H, Mirolo M, Tarik M, Kazzi M, Trabesinger S (2020) Multifunctional electrolyte additive for improved interfacial stability in Ni-rich layered oxide full-cells. Energy Storage Mater 33:216–229
8. Wang C, Yu L, Fan W, Liu J, Ouyang L, Yang L, Zhu M (2017) 3,3′-(Ethylenedioxy)dipropiononitrile as an electrolyte additive for 4.5 V $LiNi_{1/3}Co_{1/3}Mn_{1/3}O_2$/graphite cells. ACS Appl Mater Interfaces 9:9630–9639
9. Han Y, Yoo J, Yim T (2016) Distinct reaction characteristics of electrolyte additives for high-voltage lithium-ion batteries: tris(trimethylsilyl) phosphite, borate, and phosphate. Electrochim Acta 215:455–465
10. Imholt L, Röser S, Börner M, Streipert B, Rad B, Winter M, Cekic-Laskovi I (2017) Trimethylsiloxy based metal complexes as electrolyte additives for high voltage application in lithium ion cells. Electrochim Acta 235:332–339
11. Li Y, Wang K, Chen J, Zhang W, Luo X, Hu Z, Zhang Q, Xing L, Li W (2020) Stabilized high-voltage cathodes via an F-rich and Si-containing electrolyte additive. ACS Appl Mater Interfaces 12:28169–28178
12. Wang C, Tang S, Zuo X, Xiao X, Liu J, Nan J (2015) 3-(1,1,2,2-Tetrafluoroethoxy)-1,1,2,2-tetrafluoropropane as a high voltage solvent for $LiNi_{1/3}Co_{1/3}Mn_{1/3}O_2$/graphite cells. J Electrochem Soc 162:A1997–A2003
13. Wang C, Zuo X, Zhao M, Xiao X, Yu L, Nan J (2016) 1H,1H,5H-Perfluoropentyl-1,1,2,2-tetrafluoroethylether as a co-solvent for high voltage $LiNi_{1/3}Co_{1/3}Mn_{1/3}O_2$/graphite cells. J Power Sources 307:772–781
14. Xu K (2004) Nonaqueous liquid electrolytes for lithium-based rechargeable batteries. Chem Rev 104:4303–4417
15. Markevich E, Baranchugov V, Aurbach D (2006) On the possibility of using ionic liquids as electrolyte solutions for rechargeable 5 V Li ion batteries. Electrochem Commun 8:1331
16. Kang Y, Park I, Park M, Choi W, Lee S, Mun J, Choi B, Koh M, Kim D, Park K (2020) L-Tryptophan: antioxidant as a film-forming additive for a high-voltage cathode. Langmuir 36:2823–2828
17. Sun Y, Huang J, Xiang H, Liang X, Feng Y, Yu Y (2020) 2-(Trifluoroacetyl) thiophene as an electrolyte additive for high-voltage lithium-ion batteries using $LiCoO_2$ cathode. J Mater Sci Technol 55:198–202
18. Liu Q, Yang G, Liu S, Han M, Wang Z, Chen L (2019) Trimethyl borate as film-forming electrolyte additive to improve high-voltage performances. ACS Appl Mater Interfaces 11:17435–17443
19. Yang B, Zhang H, Yu L, Fan W, Huang D (2016) Lithium difluorophosphate as an additive to improve the low temperature performance of $LiNi_{0.5}Co_{0.2}Mn_{0.3}O_2$/graphite cells. Electrochim Acta 221:107–114
20. Wang C, Yu L, Fan W, Liu R, Liu J, Ouyang L, Yang L, Zhu M (2018) Enhanced high-voltage cyclability of $LiNi_{0.5}Co_{0.2}Mn_{0.3}O_2$-based pouch cells via lithium difluorophosphate introducing as electrolyte additive. J Alloys Compd 755:1–9
21. Wang C, Yu L, Fan W, Liu J, Ouyang L, Yang L, Zhu M (2018) Lithium difluorophosphate as a promising electrolyte lithium additive for high-voltage lithium-ion batteries. ACS Appl Energy Mater 1:2647–2656
22. Liu Q, Ma L, Du C, Dahn J (2018) Effects of the $LiPO_2F_2$ additive on unwanted lithium plating in lithium-ion cells. Electrochim Acta 263:237–248
23. Zhao W, Zheng G, Lin M, Zhao W, Li D, Guan X, Ji Y, Ortiz G, Yang Y (2018) Toward a stable solid-electrolyte-interfaces on nickel-rich cathodes: $LiPO_2F_2$ salt-type additive and its working mechanism for $LiNi_{0.5}Mn_{0.25}Co_{0.25}O_2$ cathodes. J Power Sources 380:149–157
24. Zheng H, Xiang H, Jiang F, Liu Y, Sun Y, Liang X, Feng Y, Yu Y (2020) Lithium difluorophosphate-based dual-salt low concentration electrolytes for lithium metal batteries. Adv Energy Mater 10:2001440
25. Shi P, Zhang L, Xiang H, Liang X, Sun Y, Xu W (2018) Lithium difluorophosphate as a dendrite-suppressing additive for lithium metal batteries. ACS Appl Mater Interfaces 10:22201–22209
26. Prakasha K, Madasamy K, Kathiresan M, Prakash A (2019) Ethylviologen hexafluorophosphate as electrolyte additive for high-voltage nickel-rich layered cathode. J Phys Chem C 123:28604–28610
27. Zheng Y, Xu N, Chen S, Liao Y, Zhong G, Zhang Z, Yang Y (2020) Construction of a stable $LiNi_{0.8}Co_{0.1}Mn_{0.1}O_2$ (NCM811) cathode interface by a multifunctional organosilicon electrolyte additive. ACS Appl Energy Mater 3:2837–2845
28. Zuo X, Zhao M, Ma X, Xiao X, Liu J, Nan J (2017) Effect of diphenyl disulfide as an additive on the electrochemical

performance of $Li_{1.2}Mn_{0.54}Ni_{0.13}Co_{0.13}O_2$/graphite batteries at elevated temperature. Electrochim Acta 245:705–714
29. Hao J, Li X, Zeng X, Li D, Mao J, Guo Z (2020) Deeply understanding the Zn anode behaviour and corresponding improvement strategies in different aqueous Zn-based batteries. Energy Environ Sci 13:3917–3949
30. Hao J, Yuan L, Ye C, Chao D, Davey K, Guo Z, Qiao S (2021) Boosting zinc electrode reversibility in aqueous electrolytes by using low-cost antisolvents. Angew Chem 133:7442–7451